Talanta Open 10 (2024) 100350

Contents lists available at ScienceDirect

Talanta Open

journal homepage: www.sciencedirect.com/journal/talanta-open

Comprehensive numerical prototyping of paper-based microfluidic devices using open-source tools

Gabriel S. Gerlero [a,b], Zahar I. Guerenstein [c], Nicolás Franck [a,d], Claudio L.A. Berli [e], Pablo A. Kler [*,a,d]

[a] Centro de Investigación de Métodos Computacionales (CIMEC, UNL–CONICET), Colectora RN 168 km 472, Santa Fe, (3000), Argentina
[b] Universidad Nacional de Rafaela, Bv. Roca 989, Rafaela, (2300), Argentina
[c] Departamento de Ingenieria Mecánica, Facultad Regional Santa Fe, Universidad Tecnológica Nacional, Lavaisse 610, Santa Fe, (3000), Argentina
[d] Departamento de Ingenieria en Sistemas de Información, Facultad Regional Santa Fe, Universidad Tecnológica Nacional, Lavaisse 610, Santa Fe, (3000), Argentina
[e] Instituto de Desarrollo Tecnológico para la Industria Quimica (INTEC, UNL–CONICET), Colectora RN 168 km 472, Santa Fe, (3000), Argentina

ARTICLE INFO

Keywords:
Paper-based microfluidics
Numerical prototyping
Computer simulations
micro-Toatal Analysys Systems
Immunoassays

ABSTRACT

Paper-based microfluidics has emerged as a promising field with diverse applications ranging from medical diagnostics to environmental monitoring. Despite significant progress in research and development, the translation of paper-based prototypes into practical end-user devices remains limited. This limitation stems from challenges related to devices not being sufficiently portable and autonomous, which paper-based microfluidics is expected to overcome. Yet for this purpose, we note the lack of comprehensive numerical modeling tools capable of simulating the intricate physicochemical phenomena involved in order to optimize the development process; hence, in this study, we introduce porousMicroTransport, a novel simulation package integrated with the open-source platform OpenFOAM®, designed to address these challenges. porousMicroTransport offers efficient solvers for fluid flow and transport phenomena in microfluidic porous media, including capillarity models and (bio)chemical reactions. Moreover, under horizontal flow conditions, porousMicroTransport application field can be extended to any porous media. We demonstrate the software's effectiveness in two example cases, showcasing its ability to accurately reproduce complex phenomena involved in paper-based devices. By virtue of being an easy-to-use and computationally efficient tool, porousMicroTransport facilitates the design and optimization of devices, potentially enabling more devices to meet the WHO's REASSURED criteria for point-of-care testing. We anticipate that this tool will accelerate the development and deployment of robust and portable diagnostic devices, bridging the gap between research and practical applications.

1. Introduction

Paper-based microfluidics is nowadays a well-established R&D field; however, the number of end-user applications is still certainly limited [1]. The success of lateral flow assays (LFA), initially developed for pregnancy tests, and more recently widely spread with the rapid test for SARS-CoV-2 detection [2], could not be replicated by any other microfluidic paper-based analytical device (μPAD) [3]. Despite the huge efforts made by the scientific community to develop μPADs to comply with the REASSURED criteria proposed by the World Health Organization (WHO) [4], at present, only a few examples are available for end users as real point-of-need testing devices [5]. Many approaches have failed to simultaneously fulfill all REASSURED criteria mainly due to a high level of dependency on extra equipment for specific and complementary tasks such as heating, driving fluids, actuating valves, incubation, and reactions, among others [6]. Including these tasks within the functionality of μPADs requires increasing the complexity of devices with the consequent challenges on design and fabrication processes.

Nevertheless, the perspective is optimistic as many researchers both in academia and companies are currently working on improving different aspects of μPADs in medical diagnosis, environmental monitoring, and food quality control—among other fields—, to perform more complex tasks while being more robust, portable, and efficient [7]. For example, in order to improve robustness and portability, there are new

* Corresponding author.
E-mail addresses: ggerlero@cimec.unl.edu.ar (G.S. Gerlero), zguerenstein@frsf.utn.edu.ar (Z.I. Guerenstein), nfranck@santafe-conicet.gov.ar (N. Franck), cberli@santafe-conicet.gov.ar (C.L.A. Berli), kler@cimec.unl.edu.ar (P.A. Kler).

https://doi.org/10.1016/j.talo.2024.100350
Received 21 February 2024; Received in revised form 7 August 2024; Accepted 22 August 2024
Available online 2 September 2024

Table 1
Summary of different characteristics of the currently available software for solving fluid flow and/or reactive transport in porous media.

Software	Open source	Unsaturated flow	Multi-scalar transport	Mechanical dispersion	Retardation coefficient	Reaction support	Ref.
COMSOL	×	✓(a)	✓	×	×	✓	[32]
Ansys	×	✓(b)	✓	×	×	✓	[33]
PFLOTRAN	✓	✓	✓	✓	✓	✓(c)	[23]
porousMultiphaseFoam	✓	✓	✓	✓	✓	×	[34]
SECUReFOAM	✓	×	✓	✓	×	×	[35]
DuMuX	✓	✓	✓	✓	×	✓	[36]
OPM	✓	✓	×	×	×	×	[37]
PorePy	✓	✓	✓	×	×	×	[38]
RichardsFoam	✓	✓(d)	×	×	×	×	[39]
porousMicroTransport	✓	✓	✓	✓	✓	✓	This work

(a) Only Van Genuchten and Brooks and Corey models available.
(b) Solved using multiphase flow with Volume of Fluid method.
(c) Multiple continuum for Reactive Transport is under development.
(d) Only Van Genuchten model available.

developments in terms of fabrication techniques and the integration with mobile telephony [5,8]. Simultaneously, in order to improve sensitivity and specificity, new detection techniques coupled with the classic colorimetric and electrochemical ones are being tested [9,10]. Moreover, by improving transport and reaction mechanisms, the limits of detection of the analytes of interest can be significantly increased [11].

The aforementioned process of optimizing fluid and solute transport, as well as reaction rates, involves the systematic characterization of different substrates [12], as well as the analytical and numerical modeling of the different phenomena involved [13]. The success of these tasks will enable innovative designs that overcome the current limitations of μPADs. Unfortunately, the amount, complexity, and strong interdependence of the different physicochemical phenomena that determine the performance of a particular μPAD, turns the production of μPAD models with accurate prediction capabilities into an extremely challenging task [14]. The phenomena involved include unsaturated fluid flow governed by capillary forces; transport of multiple solute species, including unsaturated advection, anisotropic dispersion, adsorption; and (bio)chemical reactions; all of them strongly coupled and highly non-linear [15]. Remarkably, under very basic operation conditions and for simple geometries, some analytical and numerical models can help designers determine imbibition times or reactant volumes demanded [16–18]. However, accurate and computationally efficient numerical prototypes are mandatory for the design and optimization of more sophisticated applications involving 2D complex geometries, multi-step procedures, multiple fluid inlets as well as several reacting species, automatic sequential fluid delivery, or different porous materials [19].

However, at present μPAD developers do not have any software tool available able to simulate all of the aforementioned phenomena and their interactions, particularly involving complex chemical reactions [20]. In contrast, soil, as an archetypical instance of porous media, has been simultaneously studied and modeled with a set of equations similar to that needed to model μPADs [21]. Nonetheless, soil transport properties and capillary flow models differ significantly and are not fully valid for paper [22]. One of the most powerful tools in this scenario is PFLOTRAN [23], which is open-source and highly efficient for parallel computing, but it is not yet fully adapted for paper-based microfluidics [24]. Moreover, few attempts of numerical modeling μPADs with COMSOL Multiphysics were performed, yet significant discrepancies with experimental results for unsaturated flow and scalar transport were reported. Furthermore, chemical reactions were not reported within the models solved with this proprietary software [25]. A more detailed comparison of different numerical tools available for modeling μPADs or transport in porous media is presented in Table 1.

In this work, we propose the use of porousMicroTransport, a novel package that integrates with the open-source platform OpenFOAM®. Particularly, porousMicroTransport offers highly efficient solvers for saturated and unsaturated fluid flow, including the classical capillarity models (i.e. Brooks and Corey [26] and Van Genuchten [27]) as well as some alternative ones such as those from the LET family of flow functions [22,28–30]; including the possibility for users to define their own models. Regarding the scalar transport in porous media, several mechanisms are modeled such as (un)saturated advection, Brownian diffusion, mechanical dispersion, and adsorption, as well as a general arbitrary-order chemical reaction library that enables to the modeling of different types of (bio)chemical reactions. porousMicroTransport is also easy to set up, either on top of an OpenFOAM® installation or via Docker [31], and several fully functional tutorials are available within its installation. Moreover, due to the integration of porousMicroTransport to OpenFOAM®, all the advantages of the latter platform are available for users such as native support for arbitrary 3D domains, automatic compatibility with parallel computation (which can scale up to supercomputing), and the availability of source code under a GNU GPL license. Although porousMicroTransport is targeted and optimized to numerically model μPADs, the set of equations used for modeling the fluid flow and scalar transport are based on a homogenized material paradigm (e.g. Darcy-based approach for fluid flow), consequently, the presented package, can also be useful on modelling other length-scale problems based on porous materials. Only a single restriction, or consideration must be taken into account in this sense, and is that the effects of ”non-horizontal” flow, i.e. the hydrostatic or another pressure based fluid, flow cannot be adequately represented. If such conditions can be fulfilled by the studied system, porousMicroTransport will reach valid results independently of the length scale of the porous medium.

Along this work, mathematical models for all phenomena involved are reported as well as the minimal computational details for enabling users to install porousMicroTransport and run the available tutorials. Two of such tutorials are presented here, while the comparison of the numerical results with experimental data is reported and discussed. Such tutorials include all the fluid flow, transport and chemical reactions mechanisms available in porousMicroTransport for accurate and efficient numerically prototyping of μPADs. porousMicroTransport is a powerful open-source tool for improving devices and boost the launch of devices that finally can fulfill the REASSURED criteria.

2. Mathematical modeling

2.1. Fluid flow modeling

Accurate modeling of passive capillary-based pumping in paper-based microfluidics, from simple lateral flow tests to more complex analytical devices, requires considering the flow in the unsaturated regime—i.e., solving for a scalar saturation or moisture content field that varies in space and time. Using a Darcy-based approach, unsatu-

rated capillarity-driven flow in a porous medium can be deemed governed by the moisture diffusivity equation [15]:

$$\frac{\partial\theta}{\partial t} - \nabla\cdot[D(\theta)\nabla\theta] = 0 \tag{1}$$

This is a nonlinear diffusion equation in which θ represents the moisture content and $D(\theta)$ is a moisture content–dependent diffusivity defined by an unsaturated capillary flow model. It constitutes a special case of the Richards equation of flow in porous media when gravity effects are neglected, as is the case in μPADs [16]. For the case of the LETd capillary flow model [22], the diffusivity function has the expression:

$$D(\theta) = D_{wt}\frac{S_{wp}^{L}}{S_{wp}^{L} + E\left(1 - S_{wp}\right)^{T}} \tag{2}$$

with $S_{wp} = (\theta - \theta_s)/(\theta_s - \theta_r)$, where θ_s is the material's effective porosity and θ_r is the residual moisture content, while L, E, T and θ_r are fitting parameters that characterize the solid–liquid system.

2.1.1. Exhaustible-reservoir boundary condition

A special boundary condition can be used when solving Eq. (1) to represent an inlet reservoir with a finite volume of liquid (typically a drop) that can be exhausted. These kinds of reservoirs are used to orchestrate the temporal progression necessary for automatic sequential delivery. The boundary condition behaves as follows.

Under normal flow conditions—i.e., while the reservoir has enough remaining liquid that the inflow is limited solely by Eq. (1)—, the boundary condition behaves like a Dirichlet-type condition that prescribes the value of θ; exactly as would be used to model a reservoir with infinite capacity. However, once the remaining capacity falls below the inflow predicted by the flow equation, the boundary condition switches to the Neumann type with the following expression:

$$\nabla\theta\cdot\mathbf{n} = \frac{-Q}{D(\theta)|\mathbf{S_f}|\Delta t} \tag{3}$$

where Q is the remaining volume of liquid in the reservoir, n is the boundary's normal unit vector, $\mathbf{S_f}$ is the boundary's surface area, and Δt is the current timestep.

Under this Neumann-type condition, the flow through the boundary is prescribed to be equal to the remaining capacity, in order to allow the modeled reservoir to be fully exhausted while making sure that mass is conserved.

2.2. Solute transport

The transport of every diluted chemical species in a porous medium is modeled through the mass conservation equation as follows [15]:

$$\frac{\partial R_d\theta C}{\partial t} = \nabla\cdot\left[\theta D_{\text{eff}}\nabla C\right] - \nabla\cdot[UC] + \theta F \tag{4}$$

where C is the species concentration (in terms of either mass or molar units), U is the Darcy velocity ($U = -D\nabla\theta$), R_d is a retardation factor, D_{eff} is an effective diffusivity, and F is a reaction term (c.f. Section 2.3). In this conservation equation, the left hand side represents the temporal variation rate of C, while the right hand side represents the fluxes and the generation/exhaustion.

In the temporal term, the retardation factor R_d quantifies the resistance to the movement of the dissolved species due to reversible partial adsorption onto the porous matrix, which in paper is explained by chromatographic effects [40]. It is defined as:

$$R_d = 1 + \frac{\rho_s(1 - \varepsilon_{\text{tot}})K_d}{\theta} \tag{5}$$

where ρ_s is the density of the solid material, ε_{tot} is the total porosity[1] and K_d is a species-dependent partitioning coefficient for adsorption. When K_d is zero, $R_d = 1$ and the coefficient has no effect; while the retardation effect increases as K_d grows.

When considering the diffusive flow, the effective diffusivity D_{eff} accounts for the effects of Brownian molecular diffusion and mechanical dispersion in a porous material. Its expression is [15,34]:

$$D_{\text{eff}} = \left(\frac{D_M}{\tau} + \alpha_T|V|\right)I + (\alpha_L - \alpha_T)\frac{VV}{|V|} \tag{6}$$

where I is the identity tensor and V is the true velocity of the fluid ($V = U/\theta$). D_M is the species' molecular diffusion coefficient, while τ is the diffusive tortuosity, which measures the medium's resistance to diffusion. Finally, α_T and α_L are, respectively, scalar transverse and longitudinal dispersion coefficients of the medium.

2.3. Reaction terms

porousMicroTransport bundles an implementation of a reaction library. The library supports arbitrary order reactions, following a general expression of the form:

$$n_{R_1}R_1^{p_{R_1}} + n_{R_2}R_2^{p_{R_2}} + \ldots <=> \left[k_f\right][k_r]n_{P_1}P_1^{p_{P_1}} + n_{P_2}P_2^{p_{P_2}} + \ldots \tag{7}$$

where k_f and k_r are the forward and reverse rate constants, R_i are the reactant species, P_i the product species, n_{R_i} and n_{P_i} represent the stoichiometric coefficients, and p_{R_i} and p_{P_i} the reaction exponents for reactants and products respectively. Each Eq. (7) implies a net reaction rate F given by:

$$k_f([R_1]^{p_{R_1}} + [R_2]^{p_{R_2}} + \ldots) - k_r([P_1]^{p_{P_1}} + [P_2]^{p_{P_2}} + \ldots) \tag{8}$$

which is added to the reaction term in Eq. (4) for each product species P_i, but also to each reactant species R_i with opposite sign; in both cases multiplied by the species' stoichiometric coefficient n_{P_i} or n_{R_i}.

3. Materials and methods

3.1. Software

porousMicroTransport has been developed as an add-on for OpenFOAM®, an open-source multiphysics platform for solving partial differential problems [41,42]. porousMicroTransport can either be compiled from its source code or downloaded in precompiled form as a Docker image. For compilation from source, porousMicroTransport's only requirement is a development installation of OpenFOAM® v2112 or later as distributed by OpenCFD Ltd. (Bracknell, UK). As OpenFOAM®, porousMicroTransport is open-source software available under the GNU General Public License (GPL) v3.0.

Notably, the software includes an automated test suite that can verify the correct functioning of the different solvers. The test suite is written in Python and uses asynchronous APIs in order to run separate test cases in parallel, taking maximum advantage of the available computing resources in order to achieve very reasonable execution times of less than a minute for the entire suite using common hardware. This test suite also runs automatically online within the source code repository in order to ensure that any proposed changes do not negatively impact existing functionality. This continuous integration stage also tests for compatibility with all supported OpenFOAM versions, and uploads new Docker

[1] The total porosity may differ from the effective porosity due to the existence of non-connected void structures.

images if necessary.

For its part, the user-facing definition of porousMicroTransport cases is deliberately inspired by porousMultiphaseFoam [34], another toolbox for OpenFOAM® dedicated to multiphase flow and transport (without reactions) in soil.

For more information on the installation and operation of porousMicroTransport, please refer to the online README file and/or in the supplementary material that accompanies this work.

Other software utilized for this work was ParaView (Kitware Inc., Clifton Park, N. Y., United States) for data visualization, and OpenFOAM.app [43] for running OpenFOAM® natively on macOS.

3.2. Numerical details

All solvers use the finite-volume method for discretization of the equations as implemented in OpenFOAM®. What follows is a description of certain implementation details.

3.2.1. Flow equation

Within porousMicroTransport, linearization of Eq. (1)—which, depending on the conditions and the model used for D, can be highly nonlinear—is attained via Picard's method; i.e., repeated solving of a linear form of the equation that uses the previous known value for the nonlinear variables until a known tolerance is achieved. From a previous work [22] it was demonstrated that for Whatman #1 paper, the most suitable model for unsaturated flow in terms of accuracy and computational cost is LETd model that was presented in Eq. (2). However, porousMicroTransport offers the possibility to the users to choose between several models including those classical in hydrology such as Van Genuchten, Brooks and Corey, or the complete LET model, among others. Moreover, users can also implement and test new models by defining the diffusivity functions accordingly. By default, all models include the parameters adjusted for Whatman #1 paper in [22], enabling users to directly test different preset models for such substrate.

3.2.2. Exhaustible-reservoir boundary condition

The exhaustible boundary condition is implemented as a subtype of a mixed-type boundary condition, while in practice only behaving as Dirichlet type or Neumann type at a time as described in Section 2.1.1.

For the numerical implementation of this boundary condition, one must take into account that the volume of liquid that flows into the domain in a timestep can be a very small fraction of the total volume in the reservoir (especially when small timesteps are taken). In order to avoid potential excessive error caused by floating-point arithmetic, the boundary condition keeps track of the initial volume and the "used" volume of liquid in memory as independent counts instead of using a single counter for the remaining volume.

3.2.3. Reactive transport equation

The reaction model uses an explicit numerical scheme in order to support segregated solving—i.e., the concentration of each species is solved separately. This segregated approach is conventional in OpenFOAM® and allows for more scalability than a fully-coupled solver. The segregated approach also generally forces the use of explicit numerical schemes for the reaction terms if one wishes to ensure mass conservation; although a segregated mixed implicit–explicit approach—consisting of an initial (semi-)implicit solve followed by a final explicit correction pass for mass conservation—was also tested but discarded due to performance considerations.

We note that we make no provision for iterative linearization (e.g. via Picard's or Netwon's method) of the reactive transport equation in porousMicroTransport. This is done in order to improve performance; although, compounded with the use of the explicit, segregated approach, it can be detrimental for stability in practice. For this reason, it requires careful management of the timestepping—including the rewinding of timesteps where necessary—in order to preserve accuracy, with the user being required to be mindful of the adaptive timestepping configuration for each case.

While these choices are reasonable as far as our target scenarios are concerned, we can see different implementation of the reactive transport model that includes a linearization loop, or even delegates solving for the reactions to an external stiff chemistry solver through built-in support for arbitrary reaction models.

3.2.4. Automatic timestep management

porousMicroTransport includes a modular timestep control library that can support the needs of the different solvers for the possibly concurrent phenomena of flow and reactive transport. When enabled, it automatically adjusts the timestep in order to improve performance while preserving a certain level of accuracy that can be configured independently for each phenomenon. For fluid flow, it uses the required number of Picard iterations as a proxy for the difficulty in solving Eq. (1) (where the tolerance for the Picard linearization can be set by the user); increasing, maintaining, or decreasing the timestep taken according to whether the number of iterations falls below, within, or above a target range of three to seven iterations per timestep. For the reactive transport, the user can configure a maximum bound for the concentration change in a single timestep in a single finite-volume cell (as global absolute, per-species absolute, or relative tolerance), which will be used to adjust the steps taken. In all cases, a maximum step can also be configured and will—expectedly—take precedence.

Notably, and given that the nonlinearity of the phenomena at play works against an accurate prediction of the expected change in the variables being solved for in a single timestep, the timestep control library has the ability to rewind a timestep and solve again (with a smaller step, and repeatedly if necessary) if the changes in a solved timestep would violate the configured timestepping constraints. This is different from the standard OpenFOAM solvers (e.g. those using a PIMPLE loop) which simply target a Courant number with no rewind capabilities. This means that any timestepping restrictions set by the user are always enforced; it also means that an appropriate initial timestep need not be configured by the user and can instead be left to be found automatically by the solvers.

In the code, the adaptive timestepping is implemented in the form of a class hierarchy where each phenomenon (e.g. fluid flow, reactive transport) provides its own derived class that tracks and enforces its relevant constraints.

3.2.5. Parallelism

The solvers in porousMicroTransport are compatible with parallel solving through domain decomposition and the MPI standard, a method which offers impressive scalability for complex problems.

3.3. Meshing

porousMicroTransport is compatible with any finite-volume mesh supported by OpenFOAM®. For the first validation case(Section 4.1), the mesh used is made up of 16000 prisms in a simple rectangular configuration. For the reactive mixing device discussed in Section 4.2, the mesh consisted of 80000 prisms; both were made with a natural scripting mesher included in OpenFOAM®—i.e. blockMesh. This scripted mesh enables users to easily modify the geometry (including the gap, which is particularly important in the mixer case—although any change in the layout can be applied this way) by just modifying a single line of code in the blockMeshDict configuration file. For the third case (Section 4.3), a mesh of 87325 hexahedra was generated with Simcenter STAR-CCM+ (Siemens Industry Software Inc, Plano, Texas, USA).

3.4. Numerical schemes

For the dispersion test and sequential delivery application cases (Section), the numerical schemes selected were Gauss upwind phi

Table 2
Flow parameters for Whatman No. 1 paper

Description	Symbol	Value	Ref.
Effective porosity	θ_s	0.7	[22]
Initial moisture content	θ_i	0.025	[22]
Residual moisture content	θ_r	1.985×10^{-2}	[22]
LETd L coefficient	L	$4.569 \times 10^{-}3$	[22]
LETd E coefficient	E	12930	[22]
LETd T coefficient	T	1.505	[22]
LETd D_{wt} coefficient	D_{wt}	$4.660 \times 10^{-4} m^2 s^{-1}$	[22]

Table 3
Transport parameters for Whatman No. 1 paper

Description	Symbol	Value	Ref.
Diffusive tortuosity	τ	5.29	[44]
Mechanical dispersivity	α_T, α_L	30×10^{-6} m	[45]
Total porosity	ε_{tot}	0.7	[22]
Solid matrix density	ρ_s	1611 kg/m^3	[22,46]

uncorrected (fluid flow), Gauss vanLeer (species advection), and Gauss linear corrected (species dispersion–diffusion). For the reacting mixer case (Section 4.2) the numerical schemes chosen were Gauss linear limited 0.5 (fluid flow), Gauss Minmod (species advection), and Gauss linear corrected (species dispersion–diffusion). In all cases, the linear solvers were PCG (fluid flow) and PBiCG (species transport).

3.5. Hardware

The hardware used with porousMicroTransport for this paper was as follows. The mechanical dispersion test and reacting mixer cases (Section) were run on a MacBook Air (Apple Inc., Cupertino, Calif., USA) with an M1 chip with 8 GB of system RAM, using a single process for each case. For the sequential delivery application case (Section 4.3), each case ran on a single supercomputing node equipped with two Xeon Gold 6226R (Intel Corporation, Santa Clara, Calif., USA) CPUs (for a total of 32 computing cores) and 192 GB of RAM.

4. Results and discussion

Three tutorial cases included in porousMicroTransport are presented, discussed, and compared with experimental results with the aim of demonstrating its capabilities for the numerical prototyping of complex devices. The selected examples include multiple inlets for unsaturated flow, sequential delivery–class automation using exhaustible reservoirs, multiple solutes as reactants and products—including pre-adsorbed species—, and also two different reaction mechanisms. The results obtained are compared with the experimental results present in literature to show porousMicroTransport accuracy, while its robustness is shown through the complexity of the devices and its operation. In both cases, Whatman No. 1 filter paper was used as substrate. Fluid flow and transport properties of this filter paper are listed in Tables 2 and 3, respectively.

4.1. Test case for mechanical dispersion

The first tutorial example is a showcase for mechanical dispersion with a configuration similar to the experimental setup of [45]. The rectangular device has a split inlet port. Water with a dissolved species enters from half of the inlet, while pure water enters from the other half. The purpose of this case is to introduce users to the full capabilities of porousMicroTransport through a simple, straightforward case.

A simpler variant of this case is used to automatically test the predictions of mechanical dispersion against the equations in [45] as part of the continuous integration workflow.

4.1.1. Physical properties and boundary conditions

The simulation data for reproducing this tutorial case can be found at https://github.com/gerlero/porousMicroTransport/tree/main/tutorials/moistureDiffusivityTransportFoam/dispersionTest Physical properties for the case are as shown in Tables 2 and 3, with the molecular diffusivity of the species set at 1.4476×10^{-9} m^2 s^{-1}. The case as presented uses Dirichlet boundary conditions for both concentrations (for transport) and moisture content (for fluid flow) at the inlet port on the left. For the other boundaries of the domain, the conditions for transport and flow are of Neumann type.

4.1.2. Results

The results from this case are shown in Fig. 1, which displays the concentration field after 600 s of simulated time; where flow is from left to right. The effect of mechanical dispersion can be clearly observed as the fluid moves.

Besides mechanical dispersion, the one-dimensional flow in this case serves to showcase the capabilities of porousMicroTransport for solving the nonlinear flow equation (Eq. (1)): it does so in 899 timesteps for an average of 3.17 Picard linearization iterations per timestep, with 6 timestep rewinds and adaptive steps ranging from 6.91×10^{-6} s to 2.5 s. As for computational costs, the case runs to completion in 100 s of real time.

4.2. Reactive flow in a passive mixing device

This second tutorial example discusses the numerical prototyping of a passive reactive mixer presented by Hamidon et al. [11]. In that work, the authors present a patterned hourglass structure for the coflow and mixing of two reactant species: Fe^{3+} from $FeCl_3$, and SCN^- from $KSCN$ in solution. Each diluted compound enters the flow domain through reservoirs located at the bottom of the device. Due to imbibition, both solutions flow upward while generating a parallel reactive interface where the following reaction develops:

$$Fe^{3+} + SCN^- \quad <=> \quad [k_f][k_r] FeSCN^{2+}.$$

The product of the strong covalent reaction $FeSCN^{2+}$ has a particular red color that can be measured with high-precision by using standard image processing tools.

One may add a brief perspective on the foundations and evolution of

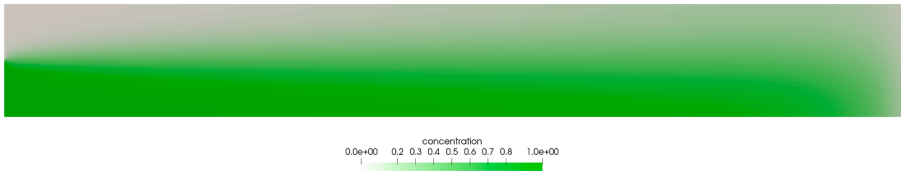

Fig. 1. Mechanical dispersion test case results as concentration field over the domain.

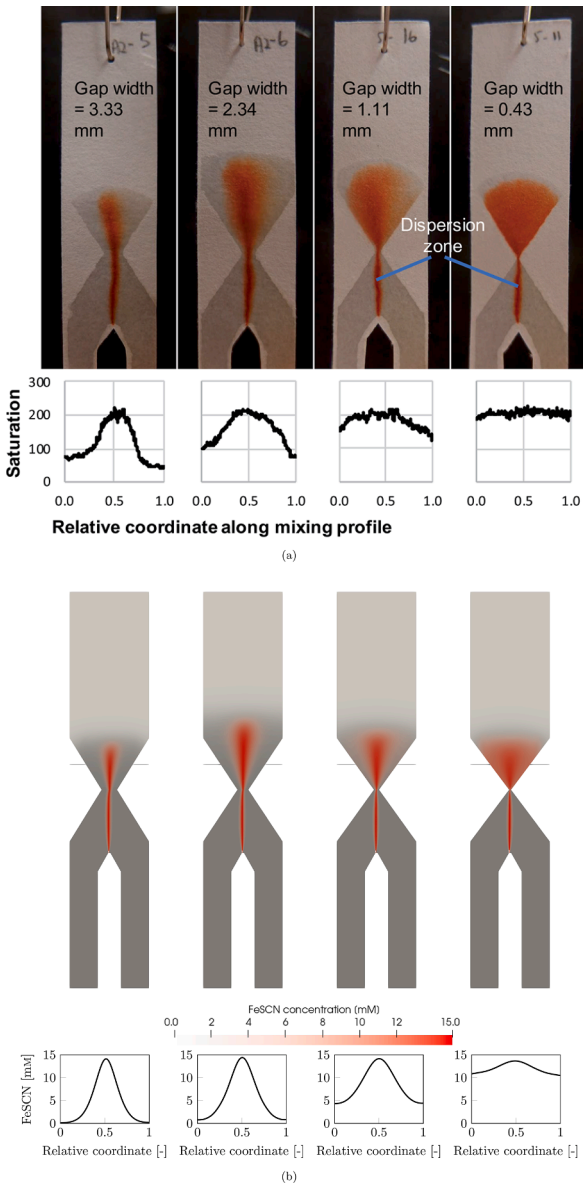

Fig. 2. (a) Experimental results from Hamidon et al. [11]; upper panel, images of the four tested devices; lower panel, distribution of the reaction product at the mixing zone. Adapted under the Creative Commons Attribution 3.0 Unported License. (b) Numerical results obtained in this work; upper panel, images of the four geometries; lower panel, distribution of the reaction product at the mixing zone (horizontal line). The grey field indicates fluid saturation.

this problem: the transverse dispersion of analytes under capillary-driven flow in paper substrates was first evaluated by Urteaga et al. [45]. Mechanical dispersion was assessed by theory and experiments, introducing a change of paradigm for the design of mixers, diluters, and concentration gradient generators on μPADs. On these foundations, the same group employed computer simulations to investigate the optimal design of paper geometries for these operations [47], where the sequence of constriction plus diffuser emerged as the best concept for mixing on paper. Later on, Verpoorte's group nicely implemented the concept to speed up reactions on paper substrates [11]. Here, we are presenting a numerical model that reproduces the entire problem for the first time, accounting for spontaneous liquid imbibition, species transport with both Brownian and mechanical dispersion, and chemical reactions. Hamidon et al. proposed the hourglass geometry with a gap of variable width in order to empirically study the mixing efficiency of the design (Fig. 2(a)). This tutorial reproduces the behavior of all of the devices manufactured by the authors to make the comparison of mixing performance. Such performance is evaluated through the color profiles determined at the gap cross section.

Table 4
Parameters for the reactive mixer tutorial case.

Description	Symbol	Value	Ref.
Inlet Fe concentration	$[Fe]_0$	50 mM	[11]
Inlet SCN concentration	$[SCN]_0$	50 mM	[11]
Molecular diffusivity Fe	$D_{M_{Fe}}$	1.45×10^{-9} m^2 s^{-1}	[48]
Molecular diffusivity SCN	$D_{M_{SCN}}$	1.77×10^{-9} m^2 s^{-1}	[48]
Forward reaction rate constant	k_f	89 M^{-1}s^{-1}	[49]
Reverse reaction rate constant	k_r	0.72 s^{-1}	[49]

4.2.1. *Physical properties and boundary conditions*

In Table 4 the transport and reaction properties of reactants are reported, as well as the concentration of every reactant at its particular inlet reservoir. All of the simulation data for reproducing this tutorial case can be found at https://github.com/gerlero/porousMicroTransport/tree/main/tutorials/moistureDiffusivityTransportFoam/reactingMixer At the reservoirs, the reported concentration is imposed as a Dirichlet boundary condition as well as the full saturation condition for the imbibition flow solver. For the other boundaries of the domain, the condition for transport and flow is a natural Neumann condition, i.e. no fluid nor solute flow in the normal direction to the boundary.

4.2.2. *Results*

Fig. 2 gathers the experimental (a) and numerical (b) results for the mixing/reactive transport process developed in the prototype proposed by Hamidon et al. [11]. In this figure, the effect of different gap widths is shown. The experimental results produced two kinds of colors. First, the grey field indicates the saturation field, and how the imbibition process developed upwards. The numerical results of the saturation field, solved through Eqs. (1) and (2), can be directly compared, showing similar results in terms of velocity of the fluid front, but also in terms of fluid front curvature. This result emphasizes the capability of porousMicroTransport to solve 2D imbibition flow in μPADs with non-trivial layout. It is noteworthy that our calculations take advantage of previous works devoted to the characterization of fluid flow and solute transport in Whatman No. 1 filter paper [22,44,45].

On the other hand, red is used to represent the concentration of the FeSCN product. When comparing the red-color profiles across all four devices, the similitude between the experimental and numerical fields for the same physical time is again remarkable. In this sense, it is important to highlight both the capability of porousMicroTransport to correctly reproduce all transport phenomena, and the fact that the transport properties and the reaction rate constants correctly characterize the experiments (Table 4).

Moreover, when focusing the analysis on the concentration profiles shown in Fig. 2 for all layouts with the aim of evaluating the mixing efficiency of each design, it can be seen that identical shapes are obtained for all cases. As it was already mentioned for the fluid flow and transport, it is clear that porousMicroTransport is able to reproduce the reaction mechanisms, but also the reaction rate constants extracted from literature. It is pertinent to emphasize here, that no arbitrary data or correction coefficient was used in the calculations: geometrical dimensions, and physicochemical parameters were directly obtained from the literature.

Regarding the numerical costs, the four cases ran simultaneously to completion in less than three hours on our hardware, which consisted of a lightweight consumer-grade laptop (c.f. Section 3.5). The analysis of results is straightforward in ParaView. It is important to compare this

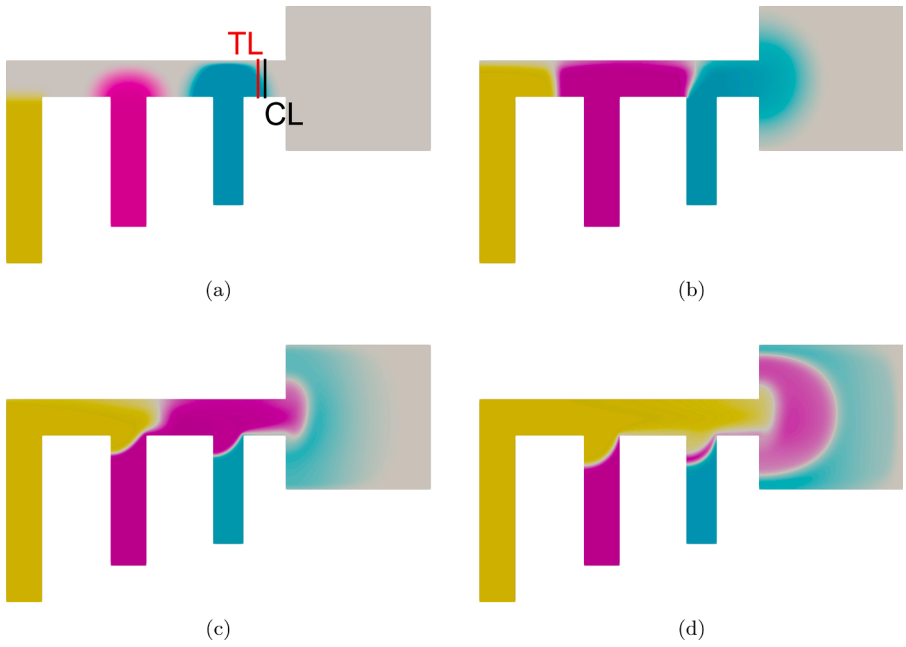

Fig. 3. Automatic delivery sequence. (a) Start of the sequence, with locations of the test (TL) and control (CL) lines highlighted. (b) First solute passes the test and control lines. (c) Second solute arrives at the test and control lines. (c) Final solute arrives.

cost with that of the experiments of the original work, upon developing every device and corresponding test. The latter costs include the manufacturing, operation, and analysis of the results, together with relatively high costs in materials and supplies, as well as qualified personnel-hours. In contrast, by using porousMicroTransport all the experimental tests can be run concurrently by a single person, on a consumer-grade computer. Furthermore, once the design and the operational sequence is optimized, a single experiment can be performed to corroborate the results, with the consequent decrease in resources and time invested in the development process.

4.3. Sequential delivery application

In this third tutorial, a paradigmatic μPAD is numerically prototyped. It is a device proposed by Fu et al. for detection of the malaria antigen *Pf*HRP2. In order to detect the aforementioned antigen, the authors proposed a kind of immunoassay known as Enzyme-Linked Immunosorbent Assay (ELISA) technique which involves several sequential steps illustrated in Fig. 3: (i) the antigen solution (green) flows over the test line (Fig. 3 (a-b)); (ii) the labeled antibody solution (pink) flows over the analyte attached to the test antibody and the control line (Fig. 3 (c)); and finally, the gold enhancement reagent flows over the two lines turning the test and control lines more visible (Fig. 3 (d)).

Table 5
Reaction rate constants for the sequential delivery application case, as obtained from Liang et al. [51].

Reaction	Forward rate constant $[M^{-1}s^{-1}]$	Dissociation rate constant $[s^{-1}]$
Eq. (9)	5×10^{7}	1.3×10^{-4}
Eq. (10)	1×10^{6}	7.1×10^{-4}
Eq. (11)	3.4×10^{3}	7.1×10^{-4}
Eq. (12)	1.6×10^{5}	2.2×10^{-3}
Eq. (13)	3.4×10^{5}	7.1×10^{-4}
Eq. (14)	3.4×10^{4}	7.1×10^{-4}
Eq. (14)	3.4×10^{5}	7.1×10^{-4}

To highlight our contributions on this problem, it is appropriate to mention that the sequential delivery of fluids for a multistep reaction had been early proposed by Fu et al. [50], who demonstrated the controlled reagent transport in disposable 2D paper networks. Then, the same group used the platform to implement heterogeneous immunoassay reactions with the format of lateral flow assays [51], where the entire process was optimized on a purely experimental basis. More recently, Rath and Toley [52] successfully implemented a computational model to describe the entire device, including relevant aspects, such as the flow through assemblies of multiple paper, species transport, and the feature of fluid reservoir with limited-volume. The numerical model we are presenting here improves on two critical aspects: (i) the prediction of the device readout in terms of test and control line product concentrations, by including the chemical reactions that take place, and (ii) the full description of species transport, by including mechanical dispersion, which is a dominant mechanism in paper substrates. Additionally, we have also tested the sequential assay concept of Liang et al. [51] in a sequential delivery format with the purpose of enhancing the output signal.

The several reactions that develop in the μPAD were modeled as follows:

$$PfHRP2 + LA \quad <=> PfHRP2LA \tag{9}$$

$$PfHRP2 + TLA \quad <=> PfHRP2TLA \tag{10}$$

$$PfHRP2LA + TLA \quad <=> PfHRP2LATLA \tag{11}$$

$$PfHRP2TLA + LA \quad <=> PfHRP2LATLA \tag{12}$$

$$PfHRP2LATLA + GER \quad <=> PfHRP2LATLAGER \tag{13}$$

$$LA + CLA \quad <=> LACLA \tag{14}$$

$$LACLA + GER \quad <=> LACLAGER \tag{15}$$

where LA corresponds to the labeled antibody, TLA and CLA to the test- and control-line antibodies respectively, and GER refers to the gold enhancement reagent. We note that in the premix case—as opposed to

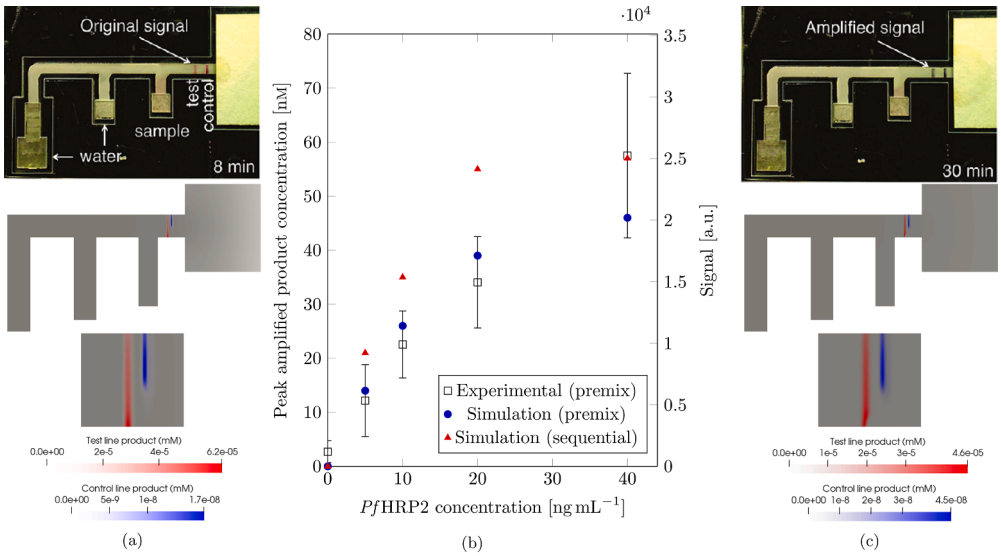

Fig. 4. (a) and (c) Visualization of unamplified and amplified (respectively) results for an analyte concentration of 200 ngm^{-1}L. Upper panels, experimental results from Fu et al. (Reprinted with permission from [53]. Copyright 2012 American Chemical Society). Lower panels, numerical results obtained in this work, along with a focus on the test and control lines. (b) Comparison of test line signals and concentrations between experimental results from Fu et al. (optical signals) and this work (product concentrations), with an additional series showing a simulated sequential format based on the work of Liang et al. [51] using this geometry.

the sequential format of Liang et al.[51]—, the reaction Eq. () do not apply.

4.3.1. Physical properties and boundary conditions

All of the simulation data for reproducing this tutorial case can be found at https://github.com/gerlero/porousMicroTransport/tree/main/tutorials/moistureDiffusivityTransportFoam/sequentialDelivery The transport properties of the antigen, antibody, and other molecules were taken from [53]. In a similar fashion to the previous case, the inlet concentrations are imposed as a Dirichlet boundary condition at the reservoirs. Regarding imbibition flow, exhaustible-reservoir boundary conditions are imposed to automatically develop the delivery sequence. Similarly, for the other boundaries of the domain, the condition for transport and fluid flow is natural Neumann condition; i.e. no fluid nor solvent flow in the normal direction to the boundary. The reaction rates are reported in Table 5.

4.3.2. Results

Fig. 4 gathers several important results of the two numerical prototypes developed in this tutorial example. The results show qualitative agreement between the unamplified and amplified products of Fig. 4(a) and (c), and simulations lie within the error bars in (b). The sequential configuration, although not experimentally tested in the sequential delivery format by Fu et al. [53], is shown to yield higher concentrations of the amplified product than the premix configuration. Each simulation case runs to completion in approximately 45 minutes using 32 concurrent processes.

5. Conclusions

In this work, we have introduced a novel open-source tool for the comprehensive numerical prototyping of μPADs named porousMicroTransport. The software is distributed as an extension for the the well-known OpenFOAM® finite volume–based multiphysics platform, inheriting all of its advantages such as arbitrary 3D mesh compatibility, parallel and supercomputing support, compatibility with high-performance data visualization, and one of the most active developer communities for open-source simulation software. It is important to stress that porousMicroTransport as it is integrated to OpenFOAM®, can be easily modified or extended in order to model another important phenomena such as heat transfer, pressure-driven flow or electrochemical detection, as well as more general length scales for the studied domains. It will also be possible in the near future to integrate porousMicroTransport with related packages aimed to electroosmotic and electrophoretic flow and transport [13].

Particularly, porousMicroTransport offers numerical capabilities for the simulation of any arbitrary μPAD layout and its different operating conditions. The numerical prototypes include saturated and unsaturated fluid flow regimes, with a collection of boundary conditions, such as fixed saturation or, exhaustible reservoir. Moreover, it includes a transport solver that includes all the known important mechanisms present in μPADs, i.e. fluid advection, Brownian diffusion, and anisotropic dispersion. Finally, it bundles a general reaction library with arbitrary order and stoichiometric coefficients. It is also continuously validated by means of an automated test suite. Finally, it should be mentioned that porousMicroTransport is also able to run seamlessly on any major operating system due to its availability as a pre-compiled Docker image.

All the aforementioned features of porousMicroTransport were demonstrated along the paper by correctly and precisely reproducing all of the phenomena involved in the tutorial examples. These tutorials were selected due to their complexity and significance for the μPAD developer community. The success of porousMicroTransport in numerically prototyping μPADs is more significant when considering the computational costs reported, that are considerably lower than the experimental time demanded for obtaining similar analyses.

With this contribution, we offer μPAD developers a very competitive numerical tool for design and optimization, to be used before and coupled to experiments in the classical iterative path from concept to product. We expect that in the near future, with the aid of porousMicroTransport, more μPADs can finally fulfill the WHO's REASSURED criteria for end users.

CRediT authorship contribution statement

Gabriel S. Gerlero: Validation, Software, Investigation, Writing – review & editing, Visualization. **Zahar I. Guerenstein:** Investigation, Data curation, Writing – original draft. **Nicolás Franck:** Methodology, Investigation, Data curation, Writing – review & editing. **Claudio L.A. Berli:** Conceptualization, Writing – review & editing, Project

administration. **Pablo A. Kler:** Conceptualization, Validation, Writing – original draft, Project administration.

Declaration of competing interest

The authors declare no financial/commercial or academic conflict of interest. The authors declare that they have no known competing financial interests or personal relationships that could have appeared to influence the work reported in this paper.

Data availability

All of the code, validation cases and application examples were developed by the authors of the work. The datasets generated and/or analyzed in the course of the current study are available at https://github.com/gerlero/porousMicroTransport.

Acknowledgements

This work was supported by CONICET, Agencia I+D+i [grant number PICT-2018-02920 and PICT-2021-00651] and UTN [grant numbers PID8132, PID8685], Argentina. The authors acknowledge Prof. Raúl Urteaga for fruitful discussions on the topic of chromatographic effects. The present work used computational resources of the Pirayu cluster, acquired with funds from the Santa Fe Science, Technology and Innovation Agency (ASACTEI), Project AC-00010-18, Resolution No. 117/14. The aforementioned equipment is part of the National High-Performance Computing System (SNCAD).

References

[1] Anushka, A. Bandopadhyay, P.K. Das, Paper based microfluidic devices: a review of fabrication techniques and applications, The European Physical Journal Special Topics 232 (6) (2023) 781–815.
[2] C.J. Toft, R.A. Bourquin, A.E. Sorenson, P.F. Horwood, J.D. Druce, P.M. Schaeffer, Analytical sensitivity of COVID-19 rapid antigen tests: A case for a robust reference standard, Talanta Open 7 (2023) 100187.
[3] N. Wang, J. Zhang, B. Xiao, A. Chen, Microfluidic-assisted integrated nucleic acid test strips for poct, Talanta (2023) 125150.
[4] D. Mabey, R.W. Peeling, A. Ustianowski, M.D. Perkins, Diagnostics for the developing world, Nature Reviews Microbiology 2 (3) (2004) 231–240.
[5] F. Schaumburg, J.P. Vidocevich, G.S. Gerlero, N. Pujato, J. Macagno, P.A. Kler, C.L. A. Berli, A free customizable tool for easy integration of microfluidics and smartphones, Scientific Reports 12 (1) (2022) 8969.
[6] J.I. Aguiar, A.O. Rangel, R.B. Mesquita, Salivary calcium determination with a specially developed microfluidic paper-based device for point-of-care analysis, Talanta Open 8 (2023) 100254.
[7] A. Sharma, B.K. Kashyap, N. Puranik, Paper-Based Diagnostic Devices for Infectious Diseases, IOP Publishing Bristol, UK, 2023.
[8] K.M. Abou El-Nour, I.M. El-Sherbiny, A.M. Abbas, E.H. Salem, G.M. Khairy, Applying smartphone camera, spectrophotometry, or ocular analysis-based dipsticks for the detection of glutathione level as a cancer biomarker, Talanta Open 7 (2023) 100211.
[9] H.A. Silva-Neto, I.V. Arantes, A.L. Ferreira, G.H. do Nascimento, G.N. Meloni, W. R. de Araujo, T.R. Paixão, W.K. Coltro, Recent advances on paper-based microfluidic devices for bioanalysis, TrAC Trends in Analytical Chemistry 158 (2023) 116893.
[10] J. Macagno, G.S. Gerlero, M.L. Satuf, C.L.A. Berli, Field-deployable aptasensor with automated analysis of stain patterns for the detection of chlorpyrifos in water, Talanta 252 (2023) 123782.
[11] N.N. Hamidon, G.I. Salentijn, E. Verpoorte, Enhanced passive mixing for paper microfluidics, RSC Advances 11 (41) (2021) 25677–25685.
[12] N. Franck, F. Schaumburg, P.A. Kler, R. Urteaga, Precise electroosmotic flow measurements on paper substrates, Electrophoresis 42 (7-8) (2021) 975–982.
[13] G.S. Gerlero, S. Marquez Damian, F. Schaumburg, N. Franck, P.A. Kler, Numerical simulations of paper-based electrophoretic separations with open-source tools, Electrophoresis 42 (16) (2021) 1543–1551.
[14] S. Modha, C. Castro, H. Tsutsui, Recent developments in flow modeling and fluid control for paper-based microfluidic biosensors, Biosensors and Bioelectronics 178 (2021) 113026.
[15] J. Bear, A.H.-D. Cheng, Modeling groundwater flow and contaminant transport volume 23, Dordrecht, Netherlands, Springer Science & Business Media, 2010.
[16] G.S. Gerlero, C.L.A. Berli, P.A. Kler, Open-source high-performance software packages for direct and inverse solving of horizontal capillary flow, Capillarity 6 (2) (2023) 31–40.
[17] E. Elizalde, R. Urteaga, C.L.A. Berli, Rational design of capillary-driven flows for paper-based microfluidics, Lab on a Chip 15 (10) (2015) 2173–2180.
[18] C.L.A. Berli, P.A. Kler, A quantitative model for lateral flow assays, Microfluidics and Nanofluidics 20 (7) (2016) 104.
[19] X. Yang, H. Sun, Y. Yang, Y. Liu, X. Li, Recent progress in multi-scale modeling and simulation of flow and solute transport in porous media, Wiley Interdisciplinary Reviews: Water 8 (6) (2021) e1561.
[20] F. Schaumburg, P.A. Kler, C.L.A. Berli, Numerical prototyping of lateral flow biosensors, Sensors and Actuators B: Chemical 259 (2018) 1099–1107.
[21] A.J. Ladd, P. Szymczak, Reactive flows in porous media: challenges in theoretical and numerical methods, Annual review of chemical and biomolecular engineering 12 (2021) 543–571.
[22] G.S. Gerlero, A.R. Valdez, R. Urteaga, P.A. Kler, Validity of capillary imbibition models in paper-based microfluidic applications, Transport in Porous Media 141 (2) (2022) 359–378.
[23] P. Lichtner, G. Hammond, C. Lu, S. Karra, G. Bisht, B. Andre, R. Mills, J. Kumar, PFLOTRAN User Manual: A massively parallel reactive flow and transport model for describing subsurface processes., 2017, (https://www.pflotran.org/).
[24] H. Berthet, H. Stone, F. Marty, B. Mercier, J. Jundt, D. Angelescu, Design and characterization of a MEMS-microfluidic sensor for rheological applications, Advanced Materials Research 74 (2009) 81–84.
[25] J. Tirapu-Azpiroz, A.F. Silva, M.E. Ferreira, W.F.L. Candela, P.W. Bryant, R.L. Ohta, M. Engel, M.B. Steiner, Modeling fluid transport in two-dimensional paper networks, Journal of Micro/Nanolithography, MEMS, and MOEMS 17 (2) (2018) 025003.
[26] R. Brooks, T. Corey, Hydraulic properties of porous media, Hydrology Papers, Colorado State University 24 (1964) 37.
[27] M.T. Van Genuchten, A closed-form equation for predicting the hydraulic conductivity of unsaturated soils, Soil Science Society of America journal 44 (5) (1980) 892–898.
[28] F. Lomeland, E. Ebeltoft, W.H. Thomas, A new versatile relative permeability correlation. Proceedings of the International Symposium of the Society of Core Analysts volume 112, 2005, pp. SCA2005–32.
[29] F. Lomeland, E. Ebeltoft, A new versatile capillary pressure correlation. Proceedings of the International Symposium of the Society of Core Analysts volume 29, 2008, pp. SCA2008–08.
[30] F. Lomeland, Overview of the LET family of versatile correlations for flow functions. Proceedings of the International Symposium of the Society of Core Analysts, 2018, pp. SCA2018–056.
[31] D. Merkel, et al., Docker: lightweight linux containers for consistent development and deployment, Linux Journal 239 (2) (2014) 2.
[32] Q. Li, K. Ito, Z. Wu, C.S. Lowry, S.P. Loheide II, COMSOL Multiphysics: A novel approach to ground water modeling, Groundwater 47 (4) (2009) 480–487.
[33] M.S. Rahman, U.K. Chakravarty, Characterizations of the paper-based microfluidic devices used for detecting fentanyl and related synthetic opioids. ASME International Mechanical Engineering Congress and Exposition volume 59360, American Society of Mechanical Engineers, 2019.V001T03A026
[34] P. Horgue, F. Renard, G.S. Gerlero, R. Guibert, G. Debenest, porousMultiphaseFoam v2107: An open-source tool for modeling saturated/unsaturated water flows and solute transfers at watershed scale, Computer Physics Communications 273 (2022) 108278.
[35] M. Icardi, E. Pescimoro, F. Municchi, J.J. Hidalgo, Computational framework for complex flow and transport in heterogeneous porous media, Engineering with Computers 39 (6) (2023) 3927–3940.
[36] T. Koch, D. Gläser, K. Weishaupt, S. Ackermann, M. Beck, B. Becker, S. Burbulla, H. Class, E. Coltman, S. Emmert, T. Fetzer, C. Grüninger, K. Heck, J. Hommel, T. Kurz, M. Lipp, F. Mohammadi, S. Scherrer, M. Schneider, G. Seitz, L. Stadler, M. Utz, F. Weinhardt, B. Flemisch, DuMu^x 3 - an open-source simulator for solving flow and transport problems in porous media with a focus on model coupling, Computers & Mathematics with Applications (2020), https://doi.org/10.1016/j.camwa.2020.02.012.
[37] A.F. Rasmussen, T.H. Sandve, K. Bao, A. Lauser, J. Hove, B. Skaflestad, R. Klöfkorn, M. Blatt, A.B. Rustad, O. Sævareid, et al., The open porous media flow reservoir simulator, Computers & Mathematics with Applications 81 (2021) 159–185.
[38] E. Keilegavlen, R. Berge, A. Fumagalli, M. Starnoni, I. Stefansson, J. Varela, I. Berre, Porepy: An open-source software for simulation of multiphysics processes in fractured porous media, Computational Geosciences 25 (2021) 243–265.
[39] L. Orgogozo, N. Renon, C. Soulaine, F. Hénon, S.K. Tomer, D. Labat, O. S. Pokrovsky, M. Sekhar, R. Ababou, M. Quintard, An open source massively parallel solver for richards equation: Mechanistic modelling of water fluxes at the watershed scale, Computer Physics Communications 185 (12) (2014) 3358–3371.
[40] N. Franck, L. Vera Candioti, G.S. Gerlero, R. Urteaga, P.A. Kler, A simple method for the assessment of electrophoretic mobility in porous media, Electrophoresis 45 (2024) 589–598.
[41] H. Jasak. Error analysis and estimation for the finite volume method with applications to fluid flows, Department of Mechanical Engineering, Imperial College of Science, Technology and Medicine, London, UK, 1996. Ph.D. thesis.
[42] H.G. Weller, G. Tabor, H. Jasak, C. Fureby, A tensorial approach to computational continuum mechanics using object-oriented techniques, Computers in Physics 12 (6) (1998) 620–631.
[43] G.S. Gerlero, OpenFOAM.app: Native OpenFOAM for macOS, accessed Feb 15, 2024, (https://github.com/gerlero/openfoam-app).
[44] N. Franck, C.L.A. Berli, P.A. Kler, R. Urteaga, Multiphysics approach for fluid and charge transport in paper-based microfluidics, Microfluidics and Nanofluidics 26 (11) (2022) 87.
[45] R. Urteaga, E. Elizalde, C.L.A. Berli, Transverse solute dispersion in microfluidic paper-based analytical devices (PADs), Analyst 143 (10) (2018) 2259–2266.

[46] F. Pena-Pereira, L. Villar-Blanco, I. Lavilla, C. Bendicho, Test for arsenic speciation in waters based on a paper-based analytical device with scanometric detection, Analytica chimica acta 1011 (2018) 1–10.
[47] F. Schaumburg, R. Urteaga, P.A. Kler, C.L.A. Berli, Design keys for paper-based concentration gradient generators, Journal of Chromatography A 1561 (2018) 83–91.
[48] G.S. Gerlero, S.M. Damián, P.A. Kler, electroMicroTransport v2107: Open-source toolbox for paper-based electromigrative separations, Computer Physics Communications 269 (2021) 108143.
[49] K.C. de Berg, The Iron(III) Thiocyanate Reaction: Research History and Role in Chemical Analysis, Springer International Publishing, Cham, 2019, pp. 71–86.
[50] E. Fu, B. Lutz, P. Kauffman, P. Yager, Controlled reagent transport in disposable 2D paper networks, Lab on a Chip 10 (7) (2010) 918–920.
[51] T. Liang, R. Robinson, J. Houghtaling, G. Fridley, S.A. Ramsey, E. Fu, Investigation of reagent delivery formats in a multivalent malaria sandwich immunoassay and implications for assay performance, Analytical chemistry 88 (4) (2016) 2311–2320.
[52] D. Rath, B.J. Toley, Modeling-guided design of paper microfluidic networks: A case study of sequential fluid delivery, ACS Sensors 6 (1) (2021) 91–99.
[53] E. Fu, T. Liang, P. Spicar-Mihalic, J. Houghtaling, S. Ramachandran, P. Yager, Two-dimensional paper network format that enables simple multistep assays for use in low-resource settings in the context of malaria antigen detection, Analytical Chemistry 84 (10) (2012) 4574–4579.

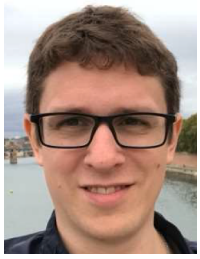

Gabriel S. Gerlero obtained a bachelor's degree in Information Systems Engineering from Universidad Tecnológica Nacional (UTN) and a PhD in Computational Mechanics from Universidad Nacional del Litoral (UNL). He is currently a postdoc at the Research Center for Computational Methods (CIMEC) in Santa Fe, Argentina. He also works as an adjunct professor at Universidad Nacional de Rafaela (UNRaf). Since 2018, he has been applying computational modeling to paper-based microfluidics. One of Gabriel's main interests is open-source software development for scientific computing.

Zahar I. Guerenstein is an undergraduate student of Mechanical Engineering at the Universidad Tecnológica Nacional (UTN), Santa Fe, Argentina. He holds a university research scholarship, working at the Research Centre for Computational Methods (CIMEC).

Nicolas Franck is a doctoral candidate at the Research Center for Computational Methods (CIMEC), at the Universidad Nacional del Litoral in Santa Fe, Argentina. He graduated with a degree in bioengineering from the National University of Entre Rios. Nicol'as research the development of paper-based electrophoretic devices for quantitative analysis. He worked on the characterization of the electroosmotic flow, of different paper substrates, modeling of porous media, and determination of electrophoretic mobilities of dyes. He is currently working on optical detection techniques for the detection of analytes of environmental interest.

Claudio L. A. Berli received a bachelor's degree in Biochemistry and PhD in Chemical Technology from National University of Litoral (UNL), Argentina. Then he held a postdoctoral position at the University of Paris, in the field of physicochemical hydrodynamics. Currently he is full professor at the Department of Basic Sciences, UNL, and Researcher of the National Council for Scientific and Technological Investigations (CONICET), at INTEC, Santa Fe, Argentina. His scientific expertise includes the fundamentals and applications of microfluidics and lab-on-a-chip devices; current research efforts are addressed to microfluidic-based drug delivery systems, as well as to accessible microfluidic technology for on-site diagnostics.

Pablo A. Kler is a research scientist at the Research Center for Computational Methods (CIMEC), at the Universidad Nacional del Litoral in Santa Fe, Argentina. He is also Associated Professor of the Informatics System Engineering department at the Universidad Tecnológica Nacional. Prof. Kler has been working since 2014 on modeling and simulations of fluid flow and reactive transport in paper-based microfludics devices with emphasis on lateral flow analysis and electromigrative separation techniques. Currently he is developing computational tools for the simulation of transport and multiphysics phenomena in porous media for biomedical, environmental, and energy applications.